Determining the contribution of volcanic ash and boundary layer aerosol in backscatter lidar returns: a three-component atmosphere approach

Article

Published Version

Determining the contribution of volcanic ash and boundary layer aerosol in backscatter lidar returns: A three-component atmosphere approach

Franco Marenco[1] and Robin J. Hogan[2]

Received 9 December 2010; revised 24 August 2011; accepted 29 August 2011; published 16 November 2011.

[1] A solution of the lidar equation is discussed, that permits combining backscatter and depolarization measurements to quantitatively distinguish two different aerosol types with different depolarization properties. The method has been successfully applied to simultaneous observations of volcanic ash and boundary layer aerosol obtained in Exeter, United Kingdom, on 16 and 18 April 2010, permitting the contribution of the two aerosols to be quantified separately. First a subset of the atmospheric profiles is used where the two aerosol types belong to clearly distinguished layers, for the purpose of characterizing the ash in terms of lidar ratio and depolarization. These quantities are then used in a three-component atmosphere solution scheme of the lidar equation applied to the full data set, in order to compute the optical properties of both aerosol types separately. On 16 April a thin ash layer, 100–400 m deep, is observed (average and maximum estimated ash optical depth: 0.11 and 0.2); it descends from ~2800 to ~1400 m altitude over a 6-hour period. On 18 April a double ash layer, ~400 m deep, is observed just above the morning boundary layer (average and maximum estimated ash optical depth: 0.19 and 0.27). In the afternoon the ash is entrained into the boundary layer, and the latter reaches a depth of ~1800 m (average and maximum estimated ash optical depth: 0.1 and 0.15). An additional ash layer, with a very small optical depth, was observed on 18 April at an altitude of 3500–4000 m. By converting the lidar optical measurements using estimates of volcanic ash specific extinction, derived from other works, the observations seem to suggest approximate peak ash concentrations of ~1500 and ~1000 μg/m^3, respectively, on the two observations dates.

Citation: Marenco, F., and R. J. Hogan (2011), Determining the contribution of volcanic ash and boundary layer aerosol in backscatter lidar returns: A three-component atmosphere approach, *J. Geophys. Res.*, *116*, D00U06, doi:10.1029/2010JD015415.

1. Introduction

[2] The April–May 2010 eruption of the Eyjafjallajökull volcano in Iceland happened during a period characterized by high atmospheric pressures over Northern Europe and the North Atlantic [*Petersen*, 2010]. This created the conditions for long-range transport of the volcanic ash plumes to Northern, Central and Southern Europe and to the Atlantic Ocean, with atmospheric residence times of the order of many days. A major air traffic disruption happened as a consequence of this [*Gertisser*, 2010]. Observations carried out during that period are of great interest for the validation and improvement of numerical dispersion models used for the prediction of volcanic ash concentrations. They have moreover proven to be a useful tool in the nearly real-time decision-making process concerning the opening or closure of airspace. Lidar has been one of the most successful remote-sensing instruments for locating the plumes: several ground-based stations have carried out observations [*Ansmann et al.*, 2010; *Flentje et al.*, 2010; *Pietruczuk et al.*, 2010; *Mona et al.*, 2011; R. J. Hogan et al., Lidar and Sun photometer retrievals of ash particle size and mass concentration from the Eyjafjallajökull volcano, manuscript in preparation, 2011] and moreover observations of volcanic ash have also been obtained by airborne lidar [*Schumann et al.*, 2011; *Marenco et al.*, 2011]. In this paper we present an inversion method useful for separately retrieving the contribution of two aerosols, using a dual-polarization backscatter lidar operating at an ultraviolet wavelength.

[3] Several papers have appeared in the last decades discussing the solution to the lidar equation for an elastic-backscattering system [see, e.g., *Fernald et al.*, 1972; *Fernald*, 1984; *Klett*, 1985; *Kovalev*, 1993; *Takamura et al.*, 1994; *Marenco et al.*, 1997; Hogan et al., manuscript in preparation, 2011]. This amount of literature is justified by the fact that the equation is underdetermined, i.e. for any measured lidar profile infinite mathematical solutions are possible, whereas only one will have to be retained as the best estimate of the state of the atmosphere. In the assumption of single elastic

[1]Observational Based Research, Met Office, Exeter, UK.
[2]Department of Meteorology, University of Reading, Reading, UK.

0148-0227/11/2010JD015415

scattering, monochromatic radiative transfer applied to lidar returns leaves us with backscatter and extinction tied together in an integral equation: with two unknowns and only one equation, insufficient information is available for finding a deterministic solution.

[4] In the absence of a definite physical principle to be used for the purpose of constraining the solution, since *Fernald et al.* [1972] the scientific community has often resorted to the assumption that the lidar ratio (extinction-to-backscatter ratio) is constant. This assumption could in principle be relaxed as in the work by *Klett* [1985] provided that the vertical profile of the lidar ratio is known, but if one is left with an elastic-backscatter lidar alone there is of course no simple way of establishing that profile. Note that on one side the assumption of a constant lidar ratio is made because there are often no other practical possibilities for inverting the lidar equation, and on the other side this seems a reasonable assumption for an aerosol layer from a given source and for which microphysical properties such as composition and particle size/shape may be assumed homogeneous.

[5] Even in the assumption of a constant lidar ratio, the lidar retrieval remains underdetermined since two parameters need be set. One of them is the value of the lidar ratio itself, and the other is the lidar calibration constant; the latter is usually determined by comparison of the signal with what is expected from a known target, most often Rayleigh scattering by an aerosol-free layer. This framework is often referred to as the Fernald-Klett approach [*Fernald*, 1984; *Klett*, 1985]. The lidar constant is usually not determined *a priori* in the laboratory, for two reasons: the first being that the laser output and receiver efficiency may vary (i.e. the lidar constant is so-called because of its independence upon range, but it still may vary with time), and the second, more fundamental, is that as shown by *Fernald* [1984] the mathematical solution is unstable for a near-range calibration, so that the reference range used for calibration must be taken at the far end of the lidar profile. In the latter case, as we proceed inward from the reference range the solution becomes more and more independent from the calibration assumptions.

[6] Note that the Fernald-Klett approach is not the only one that is based on the assumption of a constant lidar ratio. For an elastic-backscattering system two independent constrains to the lidar equation must still be given (this being required mathematically), and several approaches have appeared in the literature. *Kovalev* [1993], for instance, proposed a solution based on the knowledge of the lidar ratio and of the aerosol optical depth; *Di Girolamo et al.* [1994] used a solution based on *two* aerosol-free calibration ranges, one below and one above the aerosol layer; and *Takamura et al.* [1994]; *Marenco et al.* [1997] proposed a solution based on an independent optical depth measurement and an aerosol-free calibration range.

[7] All of the solutions to the lidar equation mentioned above are based on a two-component atmosphere, where the components are the molecular free-atmosphere (Rayleigh scattering) and the aerosols, respectively; the first component being assumed to be fully known from a model or a radiosonde profile, and the second component being assumed to have a constant lidar ratio. If distinct aerosol layers are observed at the same time, which are believed to have different properties, a two-component scheme can still be used by dividing up the lidar profiles into separate sections. This approach will however be insufficient for cases when two different aerosol types co-exist in a same atmospheric layer: if knowing in advance how the proportion of the two aerosols varies with range, one could use one of the schemes that assumes a variable lidar ratio, but this cannot be expected to work if that proportion has to be determined from the lidar observations.

[8] Other approaches to the problem exist, namely using systems such as Raman lidar [*Ferrare et al.*, 1998; *Tesche et al.*, 2009] or high spectral resolution lidar [*Shipley et al.*, 1983; *Rogers et al.*, 2009], which permit one to independently evaluate backscattering and extinction. The study of the simple elastic-backscattering lidar remains relevant, however, because many systems not featuring these additional detection channels can still provide useful information. Raman lidars are moreover strongly limited by the amount of daylight, so that some widely used systems can only be fully exploited at nighttime, whereas high resolution lidar requires hyperspectral measurements which may complicate the experimental apparatus. On the other hand, elastic-backscatter lidar (with or without depolarization) has the advantages of simplicity and lower cost, two features that encourage the development of monitoring networks.

[9] The addition of a depolarization channel has proven in many cases to be the most reliable way to distinguish volcanic ash from other, more common, aerosols, and a strong depolarization is considered a good tracer for ash [*Hoffmann et al.*, 2010; *Ansmann et al.*, 2011] and dust [*Freudenthaler et al.*, 2009; *Tesche et al.*, 2009]. In particular, the ash layers have sometimes been observed at a sufficiently high altitude, well above the boundary layer (BL) aerosol, and thus could be treated separately. At other times, however, the ash has reached the BL top, and as a consequence has mixed with the BL aerosol. In such observations, the lidar signal can be inverted into quantitative measurements (backscatter and extinction coefficients), and the depolarization signal can be separately used as a qualitative indicator to distinguish the ash from the BL aerosol background; but working within a two-component atmosphere framework it may be difficult in some scenes to quantify the contribution of both aerosol types separately.

[10] An important advance has been brought by *Sugimoto et al.* [2003] and *Tesche et al.* [2009], where an algorithm is described that permits separately quantifying the contribution of two externally mixed aerosols, once total backscatter and extinction profiles have been computed. This algorithm is optimal, for instance, for use with a Raman lidar, where the lidar ratio assumption is not needed, whereas for an elastic-backscatter lidar it relies on assuming that the two aerosol types have an identical lidar ratio.

[11] The present paper originates from the remark that if depolarization is good at identifying the contribution of ash rather than locally produced aerosols, then the depolarization information should be incorporated into the aerosol inversion scheme. As a matter of fact, having a depolarization lidar channel permits having an additional and independent equation, and thus permits including additional unknowns to the lidar problem. We take this opportunity for testing a three-component atmosphere reduction scheme, where the three components, assumed externally mixed, will be respectively: Rayleigh scattering, volcanic ash (depolarizing), and BL aerosols (assumed non-depolarizing).

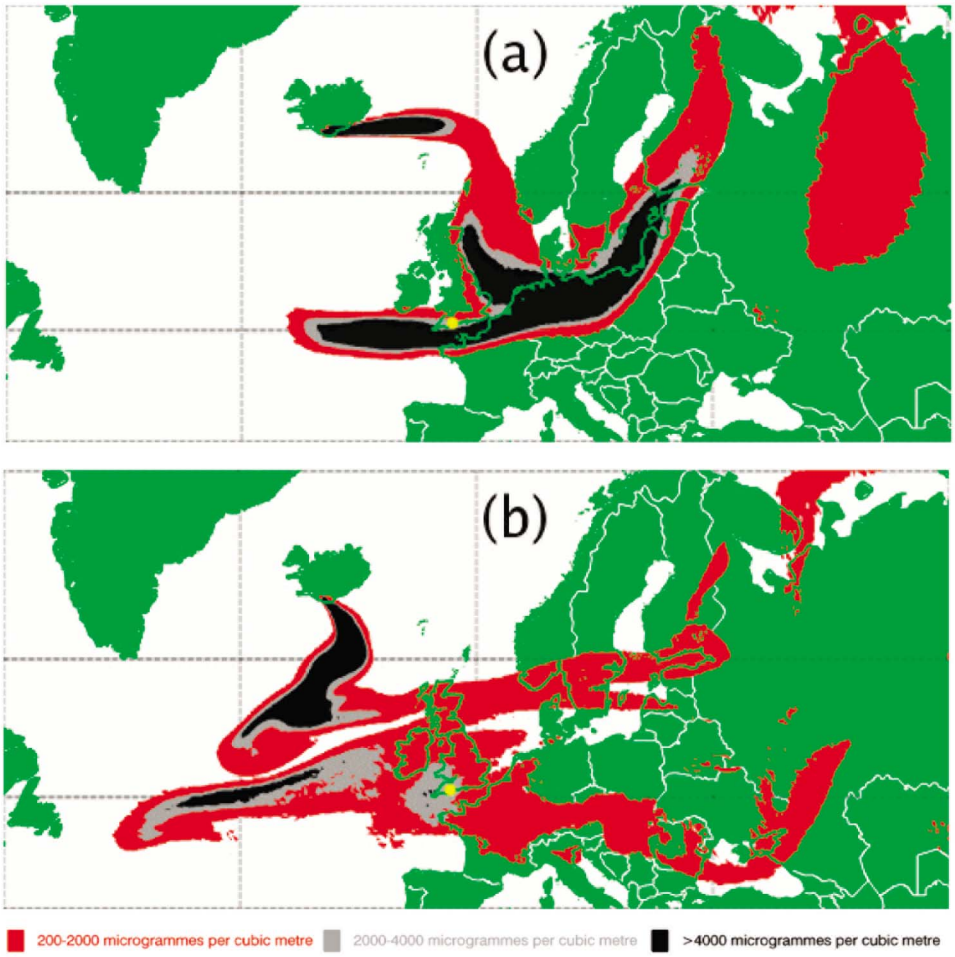

Figure 1. Volcanic ash forecasts produced with the NAME atmospheric dispersion model for 12:00 UTC on (a) 16 April and (b) 18 April: maximum ash concentration expected in the 0–6 km height level. Red 200–2000 $\mu g/m^3$; grey 2000–4000 $\mu g/m^3$; black > 4000 $\mu g/m^3$. The approximate location of Exeter is shown with a yellow dot.

[12] Section 2 describes the origin of the data; section 3 recalls the preliminary standard depolarization lidar processing that is applied throughout this article; section 4 treats selected lidar profiles, where ash is physically separated from other aerosols, in a two-component atmosphere scheme, for the purpose of characterizing volcanic ash in terms of lidar ratio and depolarization ratio; section 5 illustrates the mathematical details of the three-component atmosphere approach for externally mixed aerosols; and section 6 presents its application and results. Finally, section 7 presents a discussion of the observations and some conclusions.

2. Observations

[13] Ground-based elastic-backscattering lidar measurements were taken at Exeter (50°44′N, 3°29′W, 30 m AMSL) on 15–18 April 2010, in an effort to observe the volcanic ash plume caused by the eruption of Eyjafjallajökull; the measurements were interrupted on the evening of the 18th as the lidar was to be fitted to our research aircraft. Volcanic ash layers were observed mostly on 16 and 18 April, and discussion in this paper will focus on these two observation days for the purpose of illustrating the three-component approach. Ash dispersion forecasts produced with the Numerical Atmospheric dispersion Modeling Environment (NAME) model are shown in Figure 1. On 16 April Exeter was affected mainly by the edge of the ash plume, whereas its main part reached Central Europe [*Dacre et al.*, 2011]. On 18 April the main ash plume was expected over the Atlantic, but the whole of the United Kingdom was also expected to be affected by significative concentrations.

[14] The lidar system used is an ALS450 manufactured by Leosphere, operating at 355 nm with a 20 Hz pulse repetition frequency, and featuring a depolarization channel. Measurements were taken with a vertical resolution of 1.5 m and an integration time of 20 s, but vertical smoothing with a running average and additional integration were applied during the post-processing in order to reduce the signal-to-noise ratio. Data presented here thus have a vertical resolution of 45 m and an integration time of 1 min, except in section 4 where the data presented will have an integration time of 5 min. Local time (LT) is used throughout this paper (British summer time, UTC+1). Full overlap of the receiver field-of-

view with the emitted beam is achieved at a range of 300 m, and only data beyond this point will be considered here.

3. Range-Corrected Signal and Volume Depolarization Ratio

[15] The treatment of depolarization signals is explained by *Battan* [1973]; *Cairo et al.* [1999]; *Freudenthaler et al.* [2009]; we shall partially follow the treatment of the latter. After background subtraction and range-correction, the first step in the data treatment is the calibration of the depolarization ratio, which we do on a profile-by-profile basis in an aerosol-free region, by comparison with the depolarization of molecular scattering. We recall the equations relating the lidar signals in to atmospheric parameters for an ideal depolarization lidar:

$$P^{\parallel}(R) = K^{\parallel}\,\beta^{\parallel}(R)e^{-2\int_0^R \alpha(R)dR} \tag{1}$$

$$P^{\perp}(R) = K^{\perp}\,\beta^{\perp}(R)e^{-2\int_0^R \alpha(R)dR} \tag{2}$$

where $\beta^{\parallel}$ and $\beta^{\perp}$ are the backscattering coefficients of the atmosphere (molecules and aerosols) for the non-depolarized ($\parallel$) and depolarized ($\perp$) channels; α is the atmospheric extinction coefficient; $P^{\parallel}$ and $P^{\perp}$ are the range-corrected lidar signals for the two detection channels; $K^{\parallel}$ and $K^{\perp}$ are the lidar constants of the two channels, and R is the range. For calibrating the depolarization measurements, we must determine $K^* = K^{\perp}/K^{\parallel}$. Once this is done, it is possible to recombine the range-corrected signals:

$$P = P^{\parallel} + \frac{P^{\perp}}{K^*} \tag{3}$$

and determine the volume depolarization ratio:

$$D = \frac{P^{\perp}}{K^* P^{\parallel}}\ . \tag{4}$$

We note here that $P^{\parallel}$, $P^{\perp}$, P and D are all functions of range. Whichever of the two-component aerosol inversion schemes mentioned in the introduction is to be used, it is most accurate to use the recombined range-corrected signal in equation (3) rather than $P^{\parallel}$ alone.

[16] In practice, however, account for the cross-talk between the channels must be made, and in particular for parallel-polarized light entering the depolarized channel. This can be achieved by substituting $P^{\perp}$ in equations (3) and (4) with $P_1^{\perp} = P^{\perp} - \gamma K^* P^{\parallel}$, where γ is the cross-talk (K^* and γ being independent of range). The calibration constant is to be computed as

$$K^* = \frac{P_c^{\perp}}{P_c^{\parallel}(D_c + \gamma)}, \tag{5}$$

where $P_c^{\parallel}$ and $P_c^{\perp}$ refer to the measured range-corrected signals in a portion of the profile used for calibration, and D_c is the calibration volume depolarization ratio. A molecular portion of the profile can be selected by verifying how the signal fits a computed molecular profile, and thus it is possible to choose $D_c = \delta_m$, where δ_m is the molecular depolarization ratio. An extensive treatment of the channel cross-talk in depolarization lidar can be found in work by *Freudenthaler et al.* [2009], where more general equations are given.

[17] In the Leosphere lidar, the optical separation of the non-depolarized and depolarized channels is performed by two Brewster plates in cascade. The first plate transmits a nearly purely polarized signal which goes to the first detector, whereas the depolarized signal is reflected. As the latter is far from being pure, a second Brewster plate is used, again in reflection mode, before the signal is sent to the second detector. From the characteristics of the Brewster plates used for our lidar system, we have estimated $\gamma = 0.025$, with an uncertainty of ± 0.005.

[18] The value of δ_m is extensively discussed by *Behrendt and Nakamura* [2002], and is dependent upon the receiver bandwith. For the Leosphere lidar, the latter is 28.6 cm^{-1} (0.36 nm), and by interpolating the values given in that article, $\delta_m = 0.00415$. As we can see, $\delta_m \ll \gamma$, and the calibration in equation (5) is therefore controlled by the cross-talk more than by D_c.

[19] The latter fact can be considered positive, in the sense that the dependence of K^* upon D_c is reduced when accounting for the possibility that some small amount of depolarizing aerosol can be present at the calibration range. If, for instance, we had $D_c = 0.01$ instead of the assumed value $D_c = \delta_m$ (i.e. a more than doubled volume depolarization ratio), we would end up with an error on K^* of 17%, whereas for the same case this error would be huge in the case of an ideal lidar with $\gamma = 0$. We acknowledge that a more precise determination of γ and K^* is desirable, and that an error in their evaluation can yield a nearly proportional systematic error in the determined volume depolarization. For the future, we may set up a means to directly characterize the system with a better accuracy in the laboratory. Unfortunately, at present this characterization is unavailable.

[20] The range-corrected signal and the volume depolarization ratio for the 16 and 18 April are depicted in Figures 2 and 3. The following features are observed in the lidar range-corrected signal for 16 April: aerosol in the BL (up to 1000–1500 m); broken low level clouds between 11:00 and 18:00 LT; and a layer at higher altitude, starting at 14:00 LT a little lower than 3000 m, and slowly descending down to just above the BL. As can be observed from the bottom panel, the higher aerosol layer features a marked volume depolarization ratio, absent for the BL aerosol layer. We believe this signature to indicate its nature to be volcanic ash, and will therefore denote it as such in what follows. This assumption is justified by the synoptic analysis, which indicates an air flow from Iceland, and by the ash predictions shown in Figure 1. Clouds are rather obvious features in lidar returns, and whole vertical profiles featuring them have been removed in the bottom panel, since we want to focus on aerosol retrievals only.

[21] The 18 April data can be similarly examined from these qualitative plots. We notice a low BL aerosol layer top at the start of the day, rising up to ~1700 m in the late afternoon, with the formation of a low-level cloud for a short period around 19:00 LT. Signal from a depolarizing ash layer just above the BL is detectable in the morning until 14:00 LT, but as the BL top rises the ash loses its identity and is entrained in the BL (probably by turbulent mixing);

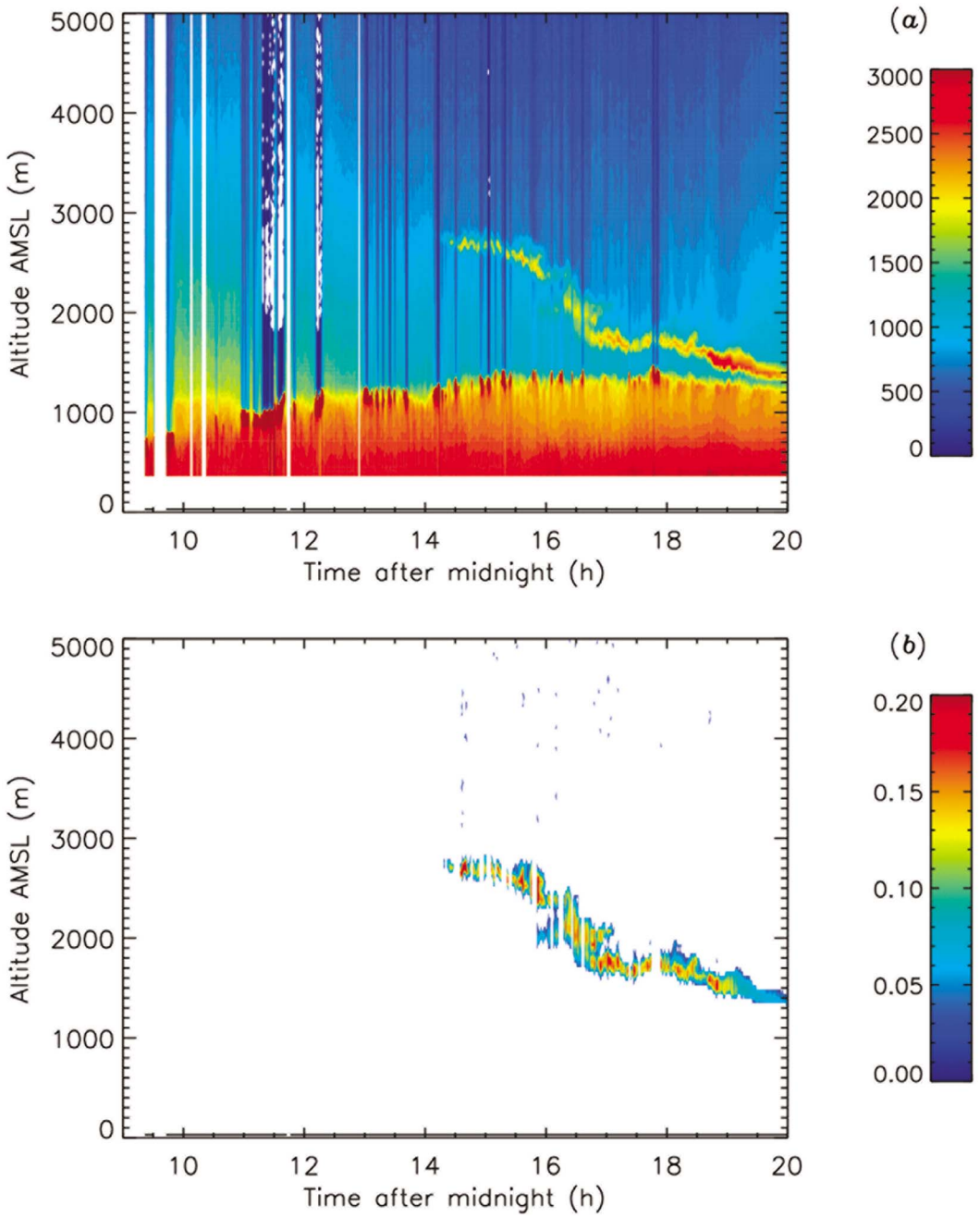

Figure 2. Lidar observations for 16 April 2010 as a function of time (UTC+1) and altitude: (a) range corrected signal (arbitrary units) and (b) volume depolarization ratio. For a better graphical rendering, volume depolarization ratios smaller than 0.02 are left blank.

the signature of the mixing is clearly seen from the depolarization panel between 14:00 and 18:00 LT. A weakly depolarizing layer is also observed for the whole duration of the observations at 3500–4000 m: we also believe this layer to be ash, but with a much smaller optical depth.

[22] In a dual-polarization lidar, the range-corrected signal and the volume depolarization ratio given by equations (3) and (4) and displayed in Figures 2 and 3 are the starting points for determining the aerosol optical properties, i.e. the aerosol backscattering coefficient, the aerosol extinction coefficient, and the aerosol depolarization ratio.

4. Characterization of Volcanic Ash

[23] In this section, we characterize volcanic ash in terms of lidar ratio and aerosol depolarization ratio, as these quantities will be needed for the three-component atmosphere method. Characterization of volcanic ash is best carried out by selecting those profiles where the ash layer

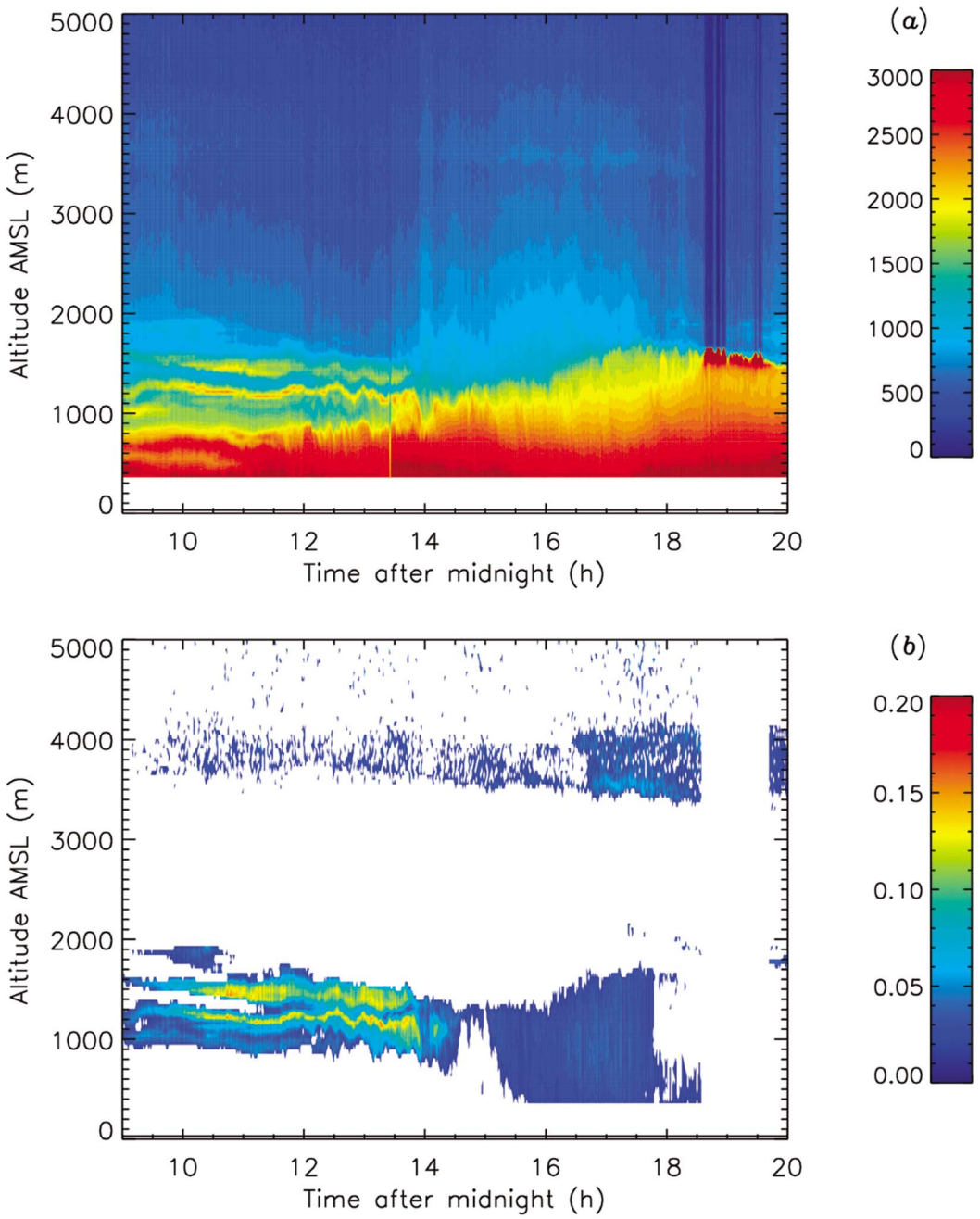

Figure 3. The same as Figure 2, but for 18 April.

yields a significant lidar signal and is at the same time clearly distinct from the BL aerosol.

[24] For this purpose, 48 profiles with a 5 min integration time have been selected from the 16 April data set; for the selected profiles no cloud disturbance is detected, and the ash layer is well above the BL aerosol, separated by a layer where molecular scattering appears dominant. The latter circumstance permits determining the optical depth of the ash layer by normalizing the lidar signal to Rayleigh scattering below and above the layer, as in *Di Girolamo et al.* [1994]. All profiles have been individually verified for fitting to a computed molecular profile in the normalization layers (see, e.g., Figure 5a). Moreover on those days infrared lidars at Cardington and Chilbolton, United Kingdom, showed no signal above the volcanic ash layers, nor between the latter and the BL aerosol (due to their wavelength, the molecular signal for these infrared lidars is too small to be detected). For these reasons we believe this normalization reasonable. By means of the double normalization, the two-component atmosphere lidar equation is fully constrained, so that the lidar ratio (assumed constant with range) and the atmospheric profiles can be determined. In order to do this we use the equations outlined by *Marenco et al.* [1997], with the difference that we are using the layer optical depth that we have determined from the lidar profile, instead of a measured optical depth from a Sun photometer.

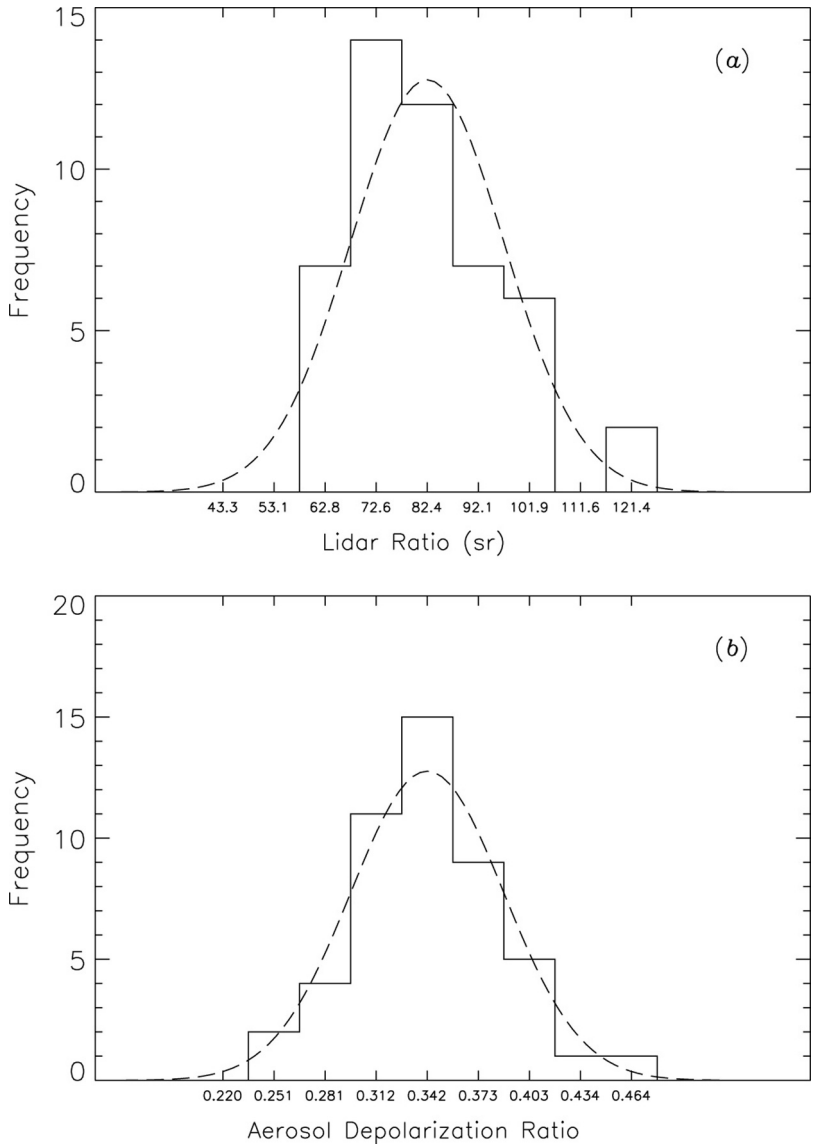

Figure 4. (a) Lidar ratio and (b) aerosol depolarization ratio for the ash layer, as determined from 48 selected 5-min integration profiles (see text). A Gaussian curve having the mean and standard deviation of the data sample is superimposed (dashed line).

[25] Once the backscatter and extinction profiles are known, we determine the aerosol depolarization ratio as in section 2.3 [*Freudenthaler et al.*, 2009]. We remind the reader that aerosol (or particle) depolarization ratio is a different quantity than volume depolarization ratio, and can only be computed after the aerosol backscatter and extinction profiles have been determined: the aerosol depolarization ratio is a property of the aerosol only, whereas the volume depolarization ratio represents the atmosphere as a whole (Rayleigh scattering and aerosols). The method for determining the aerosol depolarization ratio is fully described by *Freudenthaler et al.* [2009]. We extract a per-profile average ash depolarization ratio by averaging the aerosol depolarization ratio over the portion of the ash layer with extinction coefficient larger than half the profile maximum. At the end of this procedure, we are left with one value for the ash depolarization ratio and one for the lidar ratio for every profile. The distribution of these data is illustrated in Figure 4. The mean lidar ratio over the 48 elements is 82 sr (median 80 sr, standard deviation 15 sr) and the mean depolarization ratio is 0.342 (median 0.344, standard deviation 0.046). As the data are evenly spread around their average, we shall assume the latter as being representative of volcanic ash for the purpose of this article. This estimate of the lidar ratio is compatible with the findings from ground-based Raman lidars, although at the higher end of the observed range: *Ansmann et al.* [2010], e.g., found 55–60 sr, whereas *Mona et al.* [2011] found 40–80 sr depending on the humidity content of the ash layer.

[26] Before we continue, it is worth quantifying the uncertainty due to assuming regions above and below the aerosol layer to be purely molecular. By applying the same method but assuming in those regions an aerosol extinction coefficient of 10^{-5} m^{-1} (equivalent to 5–10% of the estimated

extinction coefficient in the BL), we derive an average lidar ratio of 65 sr (17 sr smaller than the previous result) and an average aerosol depolarization ratio of 0.400 (0.058 larger than the previous result). These possible biases have to be kept in mind in the following treatment; we limit ourselves at the moment to observing that they are not dissimilar in amplitude from the spread of the data. More discussion on uncertainties will be given in section 6.

5. Three-Component Atmosphere Approach

[27] As mentioned in the introduction, we propose a solution of the lidar equation based on three distinct atmospheric components: aerosol types 1 and 2 plus the molecular contribution m. The two aerosol types are assumed externally mixed and are to be distinguished based on depolarization. The equations for the range-corrected lidar signal P and the volume depolarization ratio D can be written as follows:

$$P = K'\left(\beta_1 + \beta_2 + \beta_m\right) e^{-2\int_{R_c}^{R}(\alpha_1+\alpha_2+\alpha_m)dR} \tag{6}$$

$$D = \frac{\frac{\delta_1\beta_1}{1+\delta_1} + \frac{\delta_2\beta_2}{1+\delta_2} + \frac{\delta_m\beta_m}{1+\delta_m}}{\frac{\beta_1}{1+\delta_1} + \frac{\beta_2}{1+\delta_2} + \frac{\beta_m}{1+\delta_m}}\ , \tag{7}$$

where $K' = K^{\|}e^{-2\int_0^{R_c}(\alpha_1+\alpha_2+\alpha_m)dR}$ is an unknown calibration parameter, R_c is a calibration range where we assume the state of the atmosphere to be known (usually molecular), β_i denotes the backscattering coefficient, α_i denotes the extinction coefficient, δ_i denotes the aerosol or molecular depolarization ratio, and i = 1, 2, m denotes the atmospheric component. In the above equations, P, D, β_i, and α_i are functions of the range R. Normalization of the contribution of each atmospheric component by $1 + \delta_i$ in both the numerator and denominator of equation (7) can be easily understood by recalling that $\delta_i = \beta_i^{\perp}/\beta_i^{\|}$ and $\beta_i = \beta_i^{\|} + \beta_i^{\perp}$.

[28] We shall assume β_m, α_m and δ_m to be fully known (see *Behrendt and Nakamura* [2002] for a characterization of δ_m), and that the two aerosol types each have a known lidar ratio $S_i = \alpha_i/\beta_i$ and a known aerosol depolarization ratio δ_i. In principle, all equations in this section could also be used with δ_1, δ_2, S_1 and S_2 being known functions of range and time, although there is no obvious method to determine those functions and thus for practical reasons we will use constants when applying the inversion scheme. As we are interested in dealing with a depolarizing (ash) and a non-depolarizing aerosol (BL), we shall assume in the following that $\delta_1 \neq 0$ and $\delta_2 = 0$, but similar (just more cumbersome) equations could be developed for the more general case, provided that $\delta_1 \neq \delta_2$. No restrictions apply to S_1 and S_2, so that they can possibly be equal; in the latter particular case an alternative resolving scheme is possible by (i) applying a Fernald-Klett aerosol retrieval, and (ii) using the method described by *Sugimoto et al.* [2003] and *Tesche et al.* [2009] to separate the two aerosols based on depolarization; the method described here deals with the more general case. From equation (7):

$$\beta_2 = \frac{\left(\frac{\delta_m}{D} - 1\right)\beta_m}{1+\delta_m} + \frac{\left(\frac{\delta_1}{D} - 1\right)\beta_1}{1+\delta_1} \tag{8}$$

and by variable substitution in equation (6):

$$P = K'\left(\beta'_m + \epsilon\beta_1\right) e^{-2\int_{R_c}^{R}(\alpha'_m+\eta\beta_1)dR}\ , \tag{9}$$

where the following can be computed from the measured volume depolarization ratio D, and are fully known functions of range:

$$\beta'_m(R) = \beta_m\left[1 + \frac{\frac{\delta_m}{D} - 1}{1+\delta_m}\right] \tag{10}$$

$$\alpha'_m(R) = \alpha_m + S_2\,\beta_m\,\frac{\frac{\delta_m}{D} - 1}{1+\delta_m} \tag{11}$$

$$\epsilon(R) = 1 + \frac{\frac{\delta_1}{D} - 1}{1+\delta_1} \tag{12}$$

$$\eta(R) = S_1 + S_2\,\frac{\frac{\delta_1}{D} - 1}{1+\delta_1}\ . \tag{13}$$

Note that the quantities defined in equations (10)–(13) are chosen because they are useful for variable substitution (they are not expected to reflect any particular physical meaning).

[29] With equation (9) we have reduced the problem to a single integral equation, with the unknown being $\beta_1(R)$; K' is an additional unknown parameter that will need setting through a boundary condition (signal normalization at the calibration range). We note that this equation is very similar to the two-component atmosphere lidar equation, and we apply to it a resolving scheme similar to the one described by *Fernald et al.* [1972]. We define

$$X_1(R) = e^{-2\int_{R_c}^{R}\eta\beta_1 dR} \tag{14}$$

and

$$X_m(R) = e^{-2\int_{R_c}^{R}\alpha'_m dR} \tag{15}$$

so that equation (9) can be rewritten as a linear first order differential equation:

$$\frac{dX_1}{dR} - \frac{2\eta\beta'_m}{\epsilon}X_1 = -\frac{2\eta P}{\epsilon K' X_m}\ , \tag{16}$$

and

$$\beta_1(R) = -\frac{1}{2\eta X_1}\frac{dX_1}{dR} = \frac{1}{\epsilon}\left(\frac{P}{K'X_mX_1} - \beta'_m\right). \tag{17}$$

[30] If we now assume that we fully know the state of the atmosphere at the calibration range R_c, then

$$K' = \frac{P_c}{\beta'_{mc} + \epsilon_c\beta_{1c}}\ , \tag{18}$$

where $P_c = P(R_c)$, $\beta'_{mc} = \beta'_m(R_c)$, $\beta_{1c} = \beta_1(R_c)$, $\epsilon_c = \epsilon(R_c)$, and $X_m(R_c) = X_1(R_c) = 1$. Note that, given the observed profile of volume depolarization, β_1 and β_2 are linked by

equation (8); therefore independent values cannot be chosen for them at the calibration range: if we wish to set $\beta_{2c} = \beta_2(R_c)$, we must accordingly compute the matching value of β_{1c}.

[31] The solution of equation (16) is as follows:

$$X_1(R) = e^{2\int_{R_c}^{R}\frac{\eta\beta'_m}{\epsilon}dR}\left\{1 - \frac{2}{K'}\int_{R_c}^{R}\frac{\eta P}{\epsilon X_m}\,e^{-2\int_{R_c}^{R}\frac{\eta\beta'_m}{\epsilon}dR}\,dR\right\}, \quad (19)$$

or in an equivalent form:

$$\beta_1(R) = \frac{1}{\epsilon}\left\{\frac{Pe^{-2\int_{R_c}^{R}\left(\frac{\eta\beta'_m}{\epsilon}-\alpha'_m\right)dR}}{\frac{P_c}{\beta'_{mc}+\epsilon_c\beta_{1c}} - 2\int_{R_c}^{R}\frac{\eta P}{\epsilon}\,e^{-2\int_{R_c}^{R}\left(\frac{\eta\beta'_m}{\epsilon}-\alpha'_m\right)dR}\,dR} - \beta'_m\right\}. \quad (20)$$

[32] This solves the problem; β_2 can be derived from equation (8) and both aerosol extinction coefficients can be derived by applying the respective lidar ratios: $\alpha_i = S_i\beta_i$. Note that the considerations on mathematical stability of the solution by *Fernald* [1984] apply to this solution as well, and a far range calibration range with inward integration will yield much better results than a near range calibration with outward integration.

6. Application of the Three-Component Method

[33] Following the characterization described in section 4, we have chosen $S_1 = 82$ sr and $\delta_1 = 0.34$ to characterize the ash. Note that this assumes that the ash optical properties are constant with time and could be a source of error in case they were not, but at the state of the art there is no practical method to overcome this assumption with a simple backscattering lidar.

[34] The second aerosol type is the BL aerosol, which we will consider non-depolarizing ($\delta_2 = 0$), as this appears reasonable from the volume depolarization ratio plots in Figures 2b, 3b, and 5d–5f. Note that the assumption $\delta_2 = 0$ for BL aerosol does not have to be regarded as general for application of the method to measurements at other times or locations; a look at the volume depolarization ratio time/height plot should however be able to give an indication in most conditions. We warn the reader that a purely non-depolarizing aerosol is in general a simplification, as any force such as drag or gravity may induce deformation of a liquid droplet. For the BL aerosol, we also set a rural (clean) continental lidar ratio, $S_2 = 35$ sr, derived from the literature [*Browell et al.*, 1985; *Omar et al.*, 2009].

[35] As with some of the other lidar inversion techniques, we have to rely on a calibration portion of the atmosphere where we believe the profile to be molecular, and apply equations (5) and (18). To minimize the influence of shot-noise on the determination of K^* and K', we actually prefer choosing a calibration *range* rather than a single calibration *point*. We therefore modify our data inversion by calculating K^* and K' for each point in the calibration range and then averaging. R_c, the point from which integration is started, is chosen as the midpoint. It is worth mentioning that we have found the solution to be more stable if both calibration ranges (used to determine K^* and K', respectively) are chosen identical. In this work, the calibration range has been chosen at 4500–5000 m as this is the lowest range where the profiles fit well to a Rayleigh scattering profile, computed accounting for scattering and extinction (for a sample, see Figures 5a–5c). Choosing the highest possible calibration range would be on one hand preferable, as we get further away from the aerosol layers, but on the other hand noise in the volume depolarization ratio increases steadily with range; this is why we have chosen to set our calibration range just after the highest aerosol layer. Moreover, as already stated in section 4, infrared lidars confirm that no aerosols are expected at this altitude.

[36] Figure 5 shows how the method works out the extinction coefficient of ash and BL aerosol separately, for three chosen vertical profiles, representative respectively of the afternoon of 16 April, and of the morning and afternoon of 18 April. In Figures 5a–5c, the range corrected signal is displayed and is compared to Rayleigh scattering profiles; in Figures 5d–5f the volume depolarization ratio is shown; and in Figures 5g–5i the result of the three-component atmosphere algorithm is displayed. It can be seen that the aerosol burden, quantified thanks to the excess lidar signal with respect to Rayleigh scattering, is split into two components according to the volume depolarization; this separation appears to be as expected.

[37] Figures 6 and 7 display the results in terms of extinction coefficient for ash and BL aerosols separately. The mixing of ash into the BL after 15:00 LT on 18 April is picked up very well, and on the same day the layer observed at 3500–4000 m also shows up in the panel displaying the ash extinction coefficient. Concerning the ash mixed in the BL, there would have been no possibility to quantify it with a traditional two-component approach (unless additional information were available) and it is in such a configuration that the three-component method displays its superiority.

[38] An estimation of the uncertainties can be obtained by perturbing the above retrievals with different assumptions on extinction at the reference calibration range and on the values of δ_1, S_1, S_2, and γ. The following sensitivity tests have been performed, one at a time, for a selection of profiles representative of the atmospheric scenes observed on the afternoon of 16 April, and on the morning and afternoon of 18 April:

[39] 1. As we have previously assumed the lidar profile to be purely molecular at the range R_c, we now do the retrieval with the three-component method but assuming an aerosol extinction coefficient of 10^{-5} m^{-1} at that same range (5–10% of the estimated extinction coefficient in the BL). As a result, the retrieved ash extinction coefficient increases by <2%. It is no sunrise to find such a small variation if one bears in mind the considerations on the stability of the solution obtained by inward integration given in *Fernald* [1984].

[40] 2. The assumed value of the volcanic ash depolarization ratio is based on previous retrievals on the same data set, as presented in section 4. In that section, it is shown that the obtained values of δ_1 display a spread of amplitude 0.05 and a possible bias of a similar magnitude; for the purpose of estimating uncertainties, we have perturbed δ_1 by ±20%; the resulting ash extinction coefficient varies by 11–17%, and its evolution is opposite in sign to the perturbation of δ_1.

[41] 3. As for δ_1, the assumed volcanic ash lidar ratio is based on our previous retrievals, and these show a spread of 15 sr and a possible bias of a similar magnitude. If we

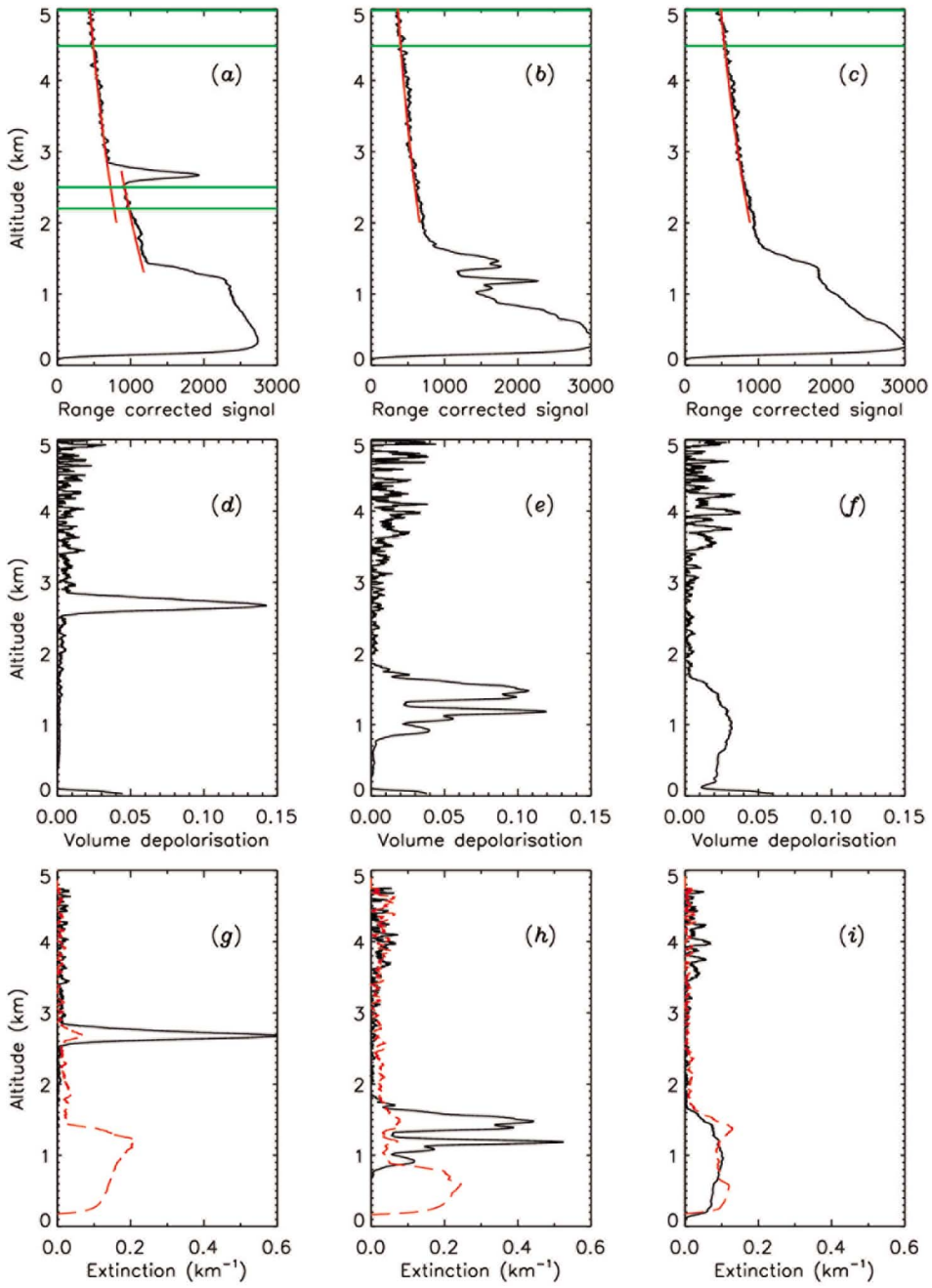

Figure 5. Example lidar profiles obtained for a 1 min integration time. (a–c) Black line, range corrected lidar signal (arbitrary units); green lines, altitude ranges believed to be molecular; red lines, Rayleigh scattering profiles fitted to the lidar signal within the molecular ranges. (d–f) Volume depolarization ratio. (g–i) Black line, volcanic ash extinction coefficient; red dashed line, BL aerosol extinction coefficient. (left) 16 April, 15:06; (middle) 18 April, 11:33; (right) 18 April, 16:28. Aerosol extinction is derived assuming a lidar ratio of 82 and 35 sr for volcanic ash and BL aerosols, respectively.

perturb S_1 by ±15 sr, we obtain a variation for the retrieved ash extinction coefficient of 15–17%; this nearly proportional variation is explained by the fact that the extinction coefficient is derived from the backscattering coefficient after multiplication by S_1.

[42] 4. Our assumed value for the BL aerosol lidar ratio, S_2, is based on the literature; we perturb this value by ±10 sr: the resulting ash extinction coefficient is little affected by this (<3%).

[43] 5. Finally, in section 3 we mentioned the possible uncertainty in γ: a bias here would affect the volume depolarization ratio almost linearly, and this is delicate since volume depolarization is at the starting point of all the retrievals that have been presented here. The average aerosol

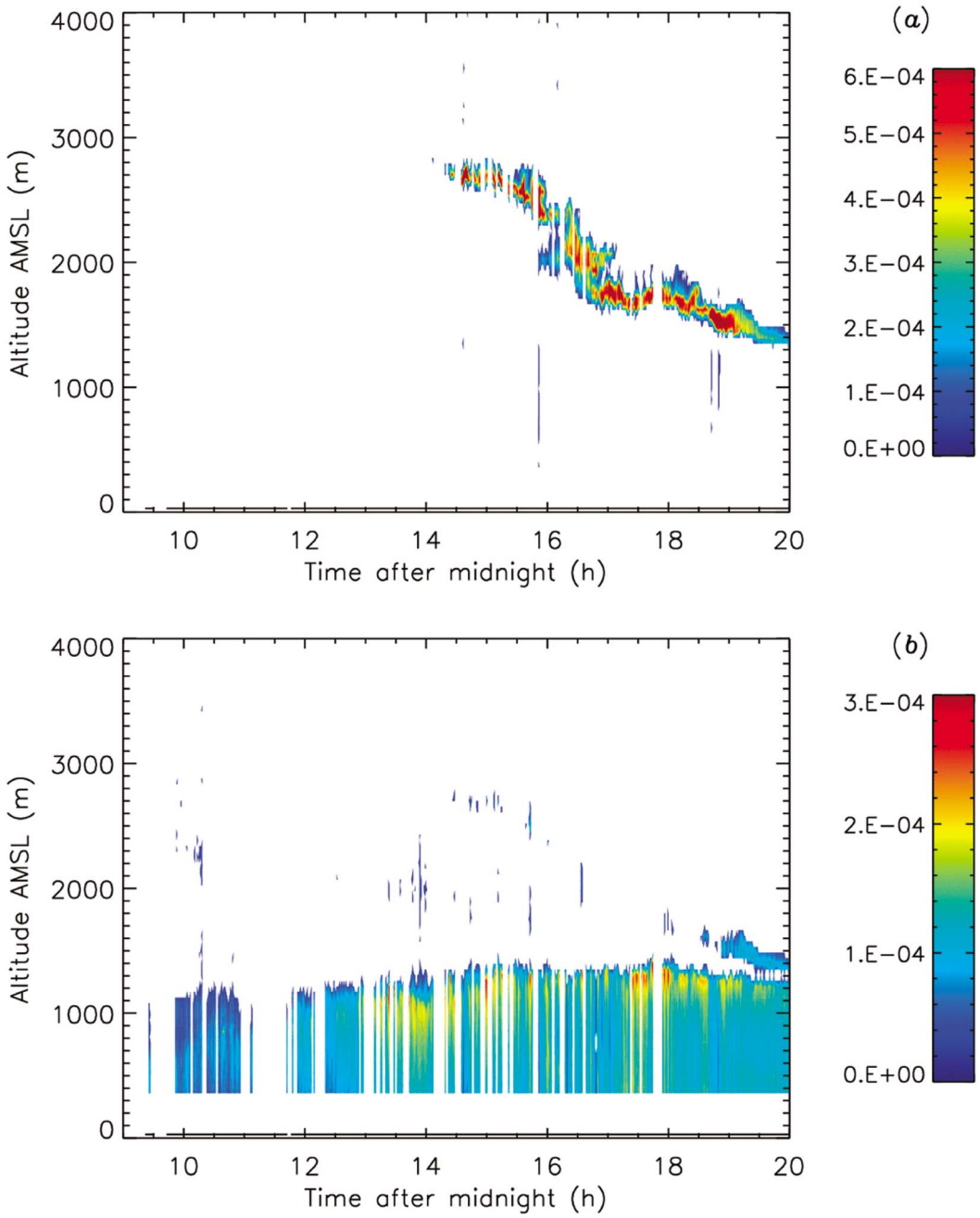

Figure 6. (a) Ash aerosol extinction coefficient and (b) boundary layer aerosol extinction coefficient on 16 April (both in m^{-1}), as a result of the three-component atmosphere inversion method. Please note that different color scales apply to Figures 6a and 6b. For a better graphical rendering, extinction coefficients smaller than $2 \cdot 10^{-5}$ m^{-1} are left blank.

depolarization ratio derived in section 4 is for instance seen to vary by ±17% when γ is perturbed by ±0.005. It is less straightforward, however, how this would affect the volcanic ash product. To be consistently investigated, the perturbation of γ has to be applied to the whole derivation in this article, i.e. the derivation of the average S_1 and δ_1 in section 4 has to be repeated, and the new values must then be used for the three-component method. The resulting variation of the volcanic ash extinction has been found very small (<2%); we explain this by the fact that errors in the two data analysis procedures cancel each other out.

[44] The above assessment of uncertainties is summarized in Table 1; when squared and combined together, they yield an overall estimated uncertainty of the order of 25% on the ash extinction coefficient.

[45] In Figure 8 we display the evolution of the aerosol optical depth (AOD) for the two aerosol components, as determined from the three-component atmosphere method

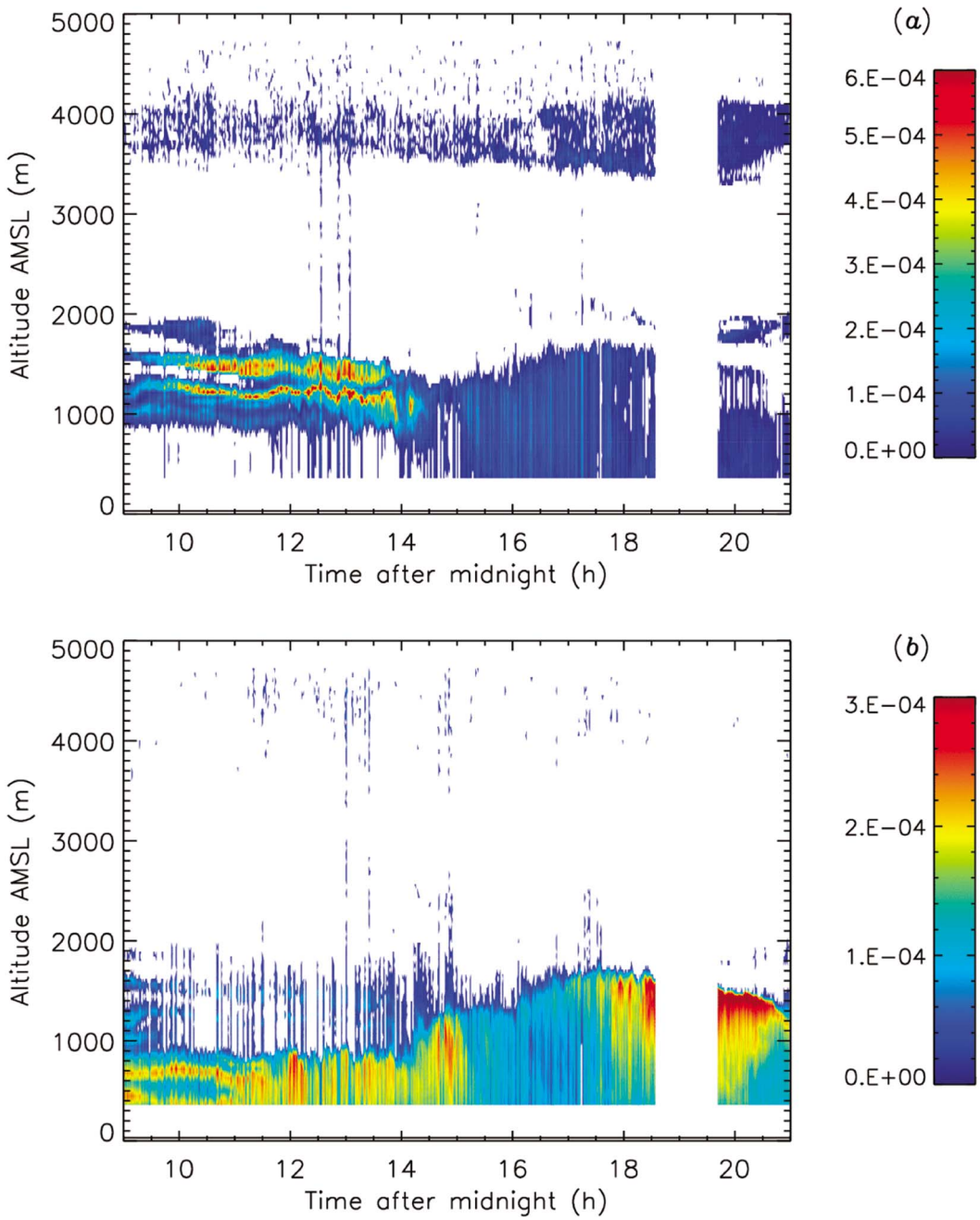

Figure 7. The same as Figure 6, but for 18 April.

Table 1. Estimation of Uncertainties Obtained by Perturbing the Assumptions Used[a]

Assumption	Perturbation	Ash Extinction Variation $\Delta\alpha_1$
Purely molecular conditions at the reference range	$\alpha_2(R_c) = 10^{-5}$ m^{-1}	+1–2%
Depolarization ratio of volcanic ash	$\delta_1 \pm 20\%$	∓11–17%
Lidar ratio of volcanic ash	$S_1 \pm 15$ sr	±15–17%
Lidar ratio of BL aerosol	$S_2 \pm 10$ sr	<3%
Estimated channel cross-talk	$\gamma \pm 0.005$	∓1–2%
Overall estimated uncertainty on the volcanic ash extinction coefficient		~25%

[a]See text for a full discussion.

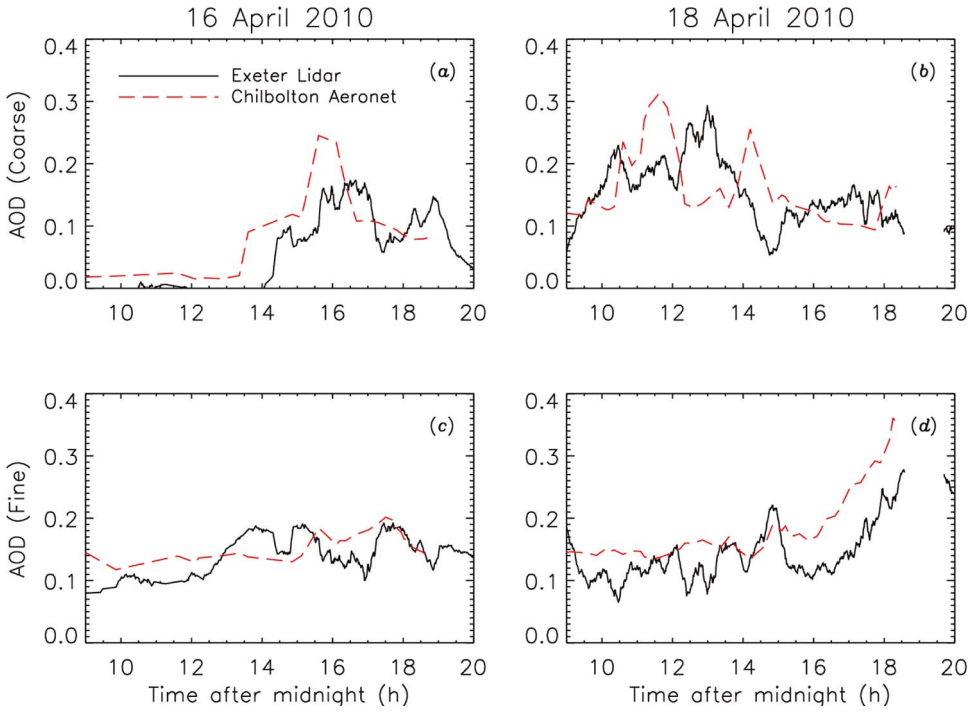

Figure 8. Aerosol optical depth (AOD) for (a, c) 16 April and (b, d) 18 April: Exeter lidar (black solid line); Chilbolton AERONET Sun photometer (red dashed line). Figures 8a and 8b depict the contribution to AOD from ash (depolarizing aerosol) at Exeter, and from the coarse particle mode at Chilbolton. Figures 8c and 8d depict contribution to AOD from the BL (non-depolarizing) aerosol at Exeter, and from the fine mode at Chilbolton.

(black solid line). As a term of comparison, we also show the AOD for coarse and fine particles at the AERONET Sun photometer station at Chilbolton, United Kingdom. When interpreting the differences between the two stations, one must account for the fact that Chilbolton is located ~150 km to the ENE of Exeter (upwind); therefore the arrival of the ash layer at Chilbolton precedes its arrival at Exeter; the delay of about an hour on 16 April is in agreement with the NAME ash dispersion model [see *Dacre et al.*, 2011]. Considering the distance between the sites, the dishomogeneity shown by the ash plume in the forecasts, and the difference in the background aerosol characteristics of the two sites, we believe that Figure 8 demonstrates a compatibility between the two data sets.

7. Discussion and Conclusions

[46] We have developed a three-component atmosphere approach to the lidar equation, and have applied it to observations featuring, after cloud screening, a depolarizing aerosol (volcanic ash) and a non-depolarizing aerosol (BL aerosol), presumed to be externally mixed. The proposed method constrains the lidar radiative transfer for a dual-polarization system, based on the assumption of known intrinsic properties for the two aerosol types (lidar ratio and aerosol depolarization ratio), and can be considered a variant of the methods by *Fernald* [1984], *Klett* [1985], and *Tesche et al.* [2009]. The three-component method seems to correctly resolve the two aerosol types and determine their individual contribution to the backscattering and extinction coefficients in this case. The implication is the possibility of isolating the contribution of volcanic ash in lidar returns, and thus of quantifying it in terms of optical properties, even in the presence of another externally mixed aerosol. After the major air traffic disruption that has followed the eruption of the Eyjafjallajökull, national authorities in some countries are considering to set up networks of ground-based lidars dedicated to ash detection and quantification, and improve their instrumented aircraft capabilities, often involving lidar as well. Moreover, ash dispersion modeling teams are in the need of quantitative data useful for tuning and assessing the prediction tools. We believe that the proposed method may represents an advance toward the meeting of these needs.

[47] On 16 April, an apparent descent of the aerosol layer with time was observed from an altitude of ~2800 m at 14:00 LT to ~1400 m at 20:00 LT, when the layer was observed just above the BL aerosol. This apparent descent is the consequence of the advection of a sloping ash layer, as documented by *Dacre et al.* [2011] and *Devenish et al.* [2011], and must not be confused with sedimentation. The average apparent descent rate over the observation period was ~200 m/h, but as a matter of fact most of the descent happened between 16:00 and 17:00 LT, at a rate of ~850 m/h, whereas both before and after that time range the rate was ~100 m/h. The ash layer was also very narrow: its depth (full width half maximum, FWHM) was as little as ~100 m before 16:00 LT, then increased to ~400 m for an hour, and then decreased again to ~150 m. It has to be remarked that the increased layer depth coincided with the faster apparent descent rate. The average and maximum aerosol optical

depths (AOD) for the ash layer were 0.11 and 0.2, respectively, with a peak extinction coefficient (maximum of the vertical distribution, computed profile by profile) ranging from $5 \cdot 10^{-4}$ to 10^{-3} m^{-1}.

[48] On 18 April a double ash layer was observed between 10:00 and 14:00 LT between 1000 and 1500 m; its apparent descent rate was quite small compared to 16 April (~30 m/h) and the ash in fact sat just above the BL top until 15:00 LT. The depth of the ash layer (FWHM) was around ~400 m; its peak extinction coefficient was 6 to $7 \cdot 10^{-4}$ m^{-1}, and its average and maximum optical depths were 0.19 and 0.27, respectively. After 14:00 LT, however, the BL depth increased as can be seen in Figure 7b, and the ash was entrained into its turbulent flow as shown in Figure 7a. The BL depth was ~1400 m at 15:00–16:00 LT and it later increased up to 1700–1800 m; it is interesting to note that although the ash extinction coefficient decreased to ~10^{-4} m^{-1}, the ash contribution to the AOD remained significant. As integrated from the lidar observations starting at a range of 300 m (full emitter/receiver overlap), the average and maximum AODs for this layer were 0.1 and 0.15, respectively (ash contribution only). Assuming a homogeneous vertical distribution from ground to 1500 m, we could estimate the ash AOD for the 0–300 m layer to be a fifth of the BL ash optical depth, and thus revise the above values by adding ~25%. An additional ash layer was observed on 18 April at 3500–4000 m; this layer was optically very thin (estimated AOD 0.02–0.04).

[49] Mass concentration estimates, which is what is required for aviation and for modeling purposes, can be derived from the extinction coefficient by application of an agreed value of the volcanic ash specific extinction. At the moment, existing estimates of the specific extinction for volcanic ash are as follows: 0.5 m^2/g [*Ansmann et al.*, 2010]; 0.4–1.2 m^2/g [*Gasteiger et al.*, 2011]; 0.64 m^2/g [*Ansmann et al.*, 2011]; 0.8 m^2/g (Hogan et al., manuscript in preparation, 2011) and 0.4–1.1 m^2/g (B. Johnson et al., In-situ observations of volcanic ash clouds from the FAAM aircraft during the eruption of Eyjafjallajökull in 2010, submitted to *Journal of Geophysical Research*, 2011). In the latter reference, the spread in the estimations is attributed to spatial and temporal variations of the ash properties, and a value of 0.6 m^2/g is given as representative of average ash conditions. Volcanic ash particles can be considered "large" compared to visible wavelengths: a typical effective radius far from the source around $r \sim 1$ μm is equivalent to a Mie scattering size parameter $x = 2\pi r/\lambda \sim 10$ (for $\lambda \sim 550$ nm). As large particles usually present an Ångström exponent near zero (geometrical optics limit [see, e.g., *Van de Hulst*, 1957]), we can consider that no significant spectral variation of the specific extinction has to be accounted for (the spectral variation of the volcanic ash specific extinction is estimated <5% by Johnson et al. (submitted manuscript, 2011)). As the ash extinction coefficient peaked at 10^{-3} m^{-1} on 16 April and $7 \cdot 10^{-4}$ m^{-1} on 18 April, we estimate the ash concentration to have peaked at ~1500 and ~1000 $\mu g/m^3$, respectively.

[50] **Acknowledgments.** Thanks to Joss Kent, Robert King and Paul Barrett for helping with the lidar operation. Thanks to the Atmospheric Dispersion Team at the Met Office for providing the volcanic ash prediction charts. Thanks to Charles Wrench for his effort in establishing and maintaining the Chilbolton AERONET site.

References

Ansmann, A., et al. (2010), The 16 April 2010 major volcanic ash plume over central Europe: EARLINET lidar and AERONET photometer observations at Leipzig and Munich, Germany, *Geophys. Res. Lett.*, *37*, L13810, doi:10.1029/2010GL043809.

Ansmann, A., et al. (2011), Ash and fine-mode particle mass profiles from EARLINET-AERONET observations over central Europe after the eruptions of the Eyjafjallajökull volcano in 2010, *J. Geophys. Res.*, *116*, D00U02, doi:10.1029/2010JD015567.

Battan, L. J. (1973), *Radar Observation of the Atmosphere*, Univ. of Chicago Press, Chicago, Ill.

Behrendt, A., and T. Nakamura (2002), Calculation of the calibration constant of polarization lidar and its dependency on atmospheric temperature, *Opt. Express*, *10*, 805–817.

Browell, E. V., S. Ismail, and S. T. Shipley (1985), Ultraviolet DIAL measurements of O_3 profiles in regions of spatially inhomogeneous aerosols, *Appl. Opt.*, *24*, 2827–2836.

Cairo, F., G. Di Donfrancesco, A. Adriani, L. Pulvirenti, and F. Fierli (1999), Comparison of various linear depolarization parameters measured by lidar, *Appl. Opt.*, *38*, 4425–4432.

Dacre, H. F., et al. (2011), Evaluating the structure and magnitude of the ash plume during the initial phase of the 2010 Eyjafjallajökull eruption using lidar observations and NAME simulations, *J. Geophys. Res.*, *116*, D00U03, doi:10.1029/2011JD015608.

Devenish, B. J., D. J. Thomson, F. Marenco, S. J. Leadbetter, and H. Ricketts (2011), A study of the arrival over the United Kingdom in April 2010 of the Eyjafjallajökull ash cloud using ground-based lidar and numerical simulations, *Atmos. Environ.*, doi:10.1016/j.atmosenv.2011.06.033, in press.

Di Girolamo, P., M. Cacciani, A. D. Sarra, G. Fiocco, and D. Fuà (1994), Lidar observations of the Pinatubo aerosol layer at Thule, Greenland, *Geophys. Res. Lett.*, *21*, 1295–1298.

Fernald, F. G. (1984), Analysis of atmospheric lidar observations: Some comments, *Appl. Opt.*, *23*, 652–653.

Fernald, F. G., B. M. Herman, and J. A. Reagan (1972), Determination of aerosol height distribution by lidar, *J. Appl. Meteorol.*, *11*, 482–489.

Ferrare, R., S. Melfi, D. Whiteman, K. Evans, and R. Leifer (1998), Raman lidar measurements of aerosol extinction and backscattering: 1. Methods and comparisons, *J. Geophys. Res.*, *103*, 19,663–19,672.

Flentje, H., H. Claude, T. Elste, S. Gilge, U. Köhler, C. Plass-Dülmer, W. Steinbrecht, W. Thomas, A. Werner, and W. Fricke (2010), The Eyiafjallajökull eruption in April 2010—Detection of volcanic plume using in-situ measurements, ozone sondes and lidar-ceilometer profiles, *Atmos. Chem. Phys.*, *10*, 10,085–10,092.

Freudenthaler, V., et al. (2009), Depolarization ratio profiling at several wavelengths in pure Saharan dust during SAMUM 2006, *Tellus, Ser. B*, *61*, 165–179.

Gasteiger, J., S. Groß, V. Freudenthaler, and M. Wiegner (2011), Volcanic ash from Iceland over Munich: Mass concentration retrieved from ground-based remote sensing measurements, *Atmos. Chem. Phys.*, *11*, 2209–2223.

Gertisser, R. (2010), Eyjafjallajökull volcano causes widespread disruption to European air traffic, *Geol. Today*, *26*, 94–95.

Hoffmann, A., C. Ritter, M. Stock, M. Maturilli, S. Eckhardt, A. Herber, and R. Neuber (2010), Lidar measurements of the Kasatochi aerosol plume in August and September 2008 in Ny-Ålesund, Spitzbergen, *J. Geophys. Res.*, *115*, D00L12, doi:10.1029/2009JD013039.

Klett, J. D. (1985), Lidar inversion with variable backscatter/extinction ratios, *Appl. Opt.*, *24*, 1638–1643.

Kovalev, V. A. (1993), Lidar measurements of the vertical aerosol extinction profiles with range-dependent backscatter-to-extinction ratios, *Appl. Opt.*, *32*, 6053–6065.

Marenco, F., V. Santacesaria, A. F. Bais, D. Balis, A. di Sarra, A. Papayannis, and C. Zerefos (1997), Optical properties of tropospheric aerosols determined by lidar and spectrophotometric measurements (Photochemical Activity and Solar Ultraviolet Radiation campaign), *Appl. Opt.*, *36*, 6875–6886.

Marenco, F., B. Johnson, K. Turnbull, S. Newman, J. Haywood, H. Webster, and H. Ricketts (2011), Airborne lidar observations of the 2010 Eyjafjallajökull volcanic ash plume, *J. Geophys. Res.*, doi:10.1029/2011JD016396, in press.

Mona, L., A. Amodeo, G. D'Amico, A. Giunta, F. Madonna, and G. Pappalardo (2011), Multi-wavelength Raman lidar observations of the Eyjafjallajökull volcanic cloud over Potenza, southern Italy, *Atmos. Chem. Phys. Discuss.*, *11*, 12,763–12,803.

Omar, A. H., et al. (2009), The CALIPSO automated aerosol classification and lidar ratio selection algorithm, *J. Atmos. Oceanic Technol.*, *26*, 1994–2014.

Petersen, G. N. (2010), A short meteorological overview of the Eyjafjallajökull eruption 14 April–23 May 2010, *Weather*, *65*, 203–207.

Pietruczuk, A., J. W. Krzyścin, J. Jaroslawski, J. Podgórski, P. Sobolewski, and J. Wink (2010), Eyjafjallajökull volcano ash observed over Belsk (52°N, 21°E), Poland, in April 2010, *Int. J. Remote Sens.*, *31*, 3981–3986.

Rogers, R. R., et al. (2009), NASA LaRC airborne high spectral resolution lidar aerosol measurements during MILAGRO: Observations and validation, *Atmos. Chem. Phys.*, *9*, 4811–4826.

Schumann, U., et al. (2011), Airborne observations of the Eyjafjalla volcano ash cloud over Europe during air space closure in April and May 2010, *Atmos. Chem. Phys.*, *11*, 2245–2279.

Shipley, S. T., D. H. Tracy, E. W. Eloranta, J. T. Tauger, J. T. Sroga, F. L. Roesler, and J. A. Weinman (1983), High spectral resolution lidar to measure optical scattering properties of atmospheric aerosols. 1: Theory and instrumentation, *Appl. Opt.*, *22*, 3716–3724.

Sugimoto, N., I. Uno, M. Nishikawa, A. Shimizu, I. Matsui, X. Dong, Y. Chen, and H. Quan (2003), Record heavy Asian dust in Beijing in 2002: Observations and model analysis of recent events, *Geophys. Res. Lett.*, *30*(12), 1640, doi:10.1029/2002GL016349.

Takamura, T., Y. Sasanu, and T. Hayasaka (1994), Tropospheric aerosol optical properties derived from lidar, Sun photometer, and optical particle counter measurements, *Appl. Opt.*, *33*, 7132–7140.

Tesche, M., A. Ansmann, D. Müller, D. Althausen, R. Engelmann, V. Freudenthaler, and S. Groß (2009), Vertically resolved separation of dust and smoke over Cape Verde using multiwavelength Raman and polarization lidars during Saharan Mineral Dust Experiment 2008, *J. Geophys. Res.*, *114*, D13202, doi:10.1029/2009JD011862.

Van de Hulst, H. C. (1957), *Light Scattering by Small Particles*, John Wiley, New York.

R. J. Hogan, Department of Meteorology, University of Reading, Earley Gate, PO Box 243, Reading RG6 6BB, UK.

F. Marenco, Observational Based Research, Met Office, Fitzroy Road, Exeter EX1 3PB, UK. (+44-1392-885393, http://www.metoffice.gov.uk/research/people/franco-marenco)